PCCP

PAPER

View Article Online
View Journal | View Issue

Cite this: *Phys. Chem. Chem. Phys.*, 2020, **22**, 5711

Enhanced piezoelectric and acoustic performances of poly(vinylidene fluoride-trifluoroethylene) films for hydroacoustic applications

Zhenji Zhou,†[a] Jinglei Li,†[ab] Weimin Xia,*[a] Xuan Zhu,[c] Tao Sun,[d] Congjun Cao[a] and Lin Zhang*[b]

Received 3rd December 2019,
Accepted 10th February 2020

DOI: 10.1039/c9cp06553a

rsc.li/pccp

Concerning the study of flexible piezoelectric devices, both scholars and engineers propose that poly(vinylidene fluoride-trifluoroethylene) (P(VDF-TrFE)) shows more merits than oriented polyvinylidene fluoride (OPVDF) in terms of dielectric, piezoelectric, mechanic–electric, acoustic emission reception performances, *etc.* Thus, in this study, to clarify the differences between the two types of polymers on their ferroelectric and piezoelectric behaviors, we systematically investigated samples to analyze their molecular structures and phase structures, and to compare their dielectric properties and acoustic emission reception performances. It was found that the wedge effect of TrFE, P(VDF-TrFE), possesses higher regular β phase crystal grains, which are easier to order along the electric field and possess more ordered static charge distribution than that of OPVDF. Consequently, a considerable saturated electric polarization (P_m ~ 15 μC cm^{-2} under 225 MV m^{-1}), a large piezoelectric coefficient (d_{33} ~ −21.5 pC N^{-1}) and a low coercive electric field (E_c ~ 50 MV m^{-1}) were obtained in the P(VDF-TrFE) films. It is worth noting that P(VDF-TrFE) shows a more stable d_{33} piezoelectric response (up to 120 °C) than that of the OPVDF. Additionally, the P(VDF-TrFE) piezoelectric films exhibit a sensitive acoustic emission reception property at approximately 70 dB and an extensive response frequency range from 10 to 100 kHz. These combined properties demonstrate that P(VDF-TrFE) piezoelectric films are a promising material for flexible and easily shaped electronic devices, including hydroacoustic sensors, actuators, and energy transfer units.

1 Introduction

Oriented polyvinylidene fluoride (OPVDF) has been widely used in various ferroelectric and piezoelectric engineering areas for its unique characteristics, including flexibility, ease of fabrication in various dimensions, relatively high piezoelectric properties, and a high electrically induced strain value.[1–3] Through uniaxial orientation, the –$(CF_2$–$CH_2)_n$– molecular chains are straightened, and the PVDF films are forced to undergo a phase transition from a nonpolar α phase (TGTG, T is *trans* and G is *gauche*) or low polar γ phase (T_3GT_3G') to an all *trans* β (TTTT) molecular conformation.[4–7] Then, the straightened molecular chains arrange into crystal-like domains, which have a strongly spontaneous polarity.[3,8] When a high electric field is applied, OPVDF piezoelectrics show a considerable piezoelectric coefficient (d_{31} ~ 20 pC N^{-1} and d_{33} ~ −20 pC N^{-1}).[8] Nowadays, OPVDF films and the related small energy transfer devices have been well investigated and commercially fabricated (*i.e.* Measurement Specialties Co. Ltd, USA and Daikin Co. Ltd, Japan) for different applications, such as in energy storage devices,[9–12] sensors,[13–17] actuators,[18] and transducers.[19,20] However, many researchers recently found that the straightened molecular chains of OPVDF tend to disorient from the β phase conformation under harsh circumstances.[21–25] As a result, the d_{33} of OPVDF decreased dramatically with increasing temperature, pressure, and storage time, before eventually losing its piezoelectric performance.[26–28] The reason for this is the straightened molecular chain with an all *trans* conformation is in a minimal entropy state which is unstable and can easily move into other irregular conformations.[29–31]

Besides OPVDF, poly(vinylidene fluoride-trifluoroethylene) (P(VDF-TrFE)) is another highly reported ferroelectric polymer that is obtained by introducing a certain proportion (20–50 mol%) of a second monomer trifluoroethylene (TrFE) into PVDF.

[a] *Xi'an University of Technology, Faculty of Printing, Packaging, and Digital Media Technology, Xi'an 710048, Shaanxi, China. E-mail: xiaweimin@xaut.edu.cn*
[b] *Electronic Materials Research Laboratory, Key Laboratory of the Ministry of Education & International Center for Dielectric Research, School of Electronic Science and Engineering, Faculty of Electronic and Information Engineering, Xi'an Jiaotong University, Xi'an, 710049, China. E-mail: zhanglin.materials@gmail.com*
[c] *Department of Civil and Environmental Engineering, the University of Utah, Salt Lake City, Utah, 84112, USA*
[d] *Media Lab, Massachusetts Institute of Technology, Cambridge, Massachusetts 02139, USA*
† These authors contributed equally.

In this way, the conformation of the PVDF is changed, and P(VDF-TrFE) possesses a spontaneous β phase regardless of the shaping conditions, which was first disclosed by Lovinger's and Tamemoto's groups.[32,33] The inserted monomer can not only improve the crystal property of PVDF but also block the stability of the kinetical form of the C–C chains in a TGTG′ conformation. Therefore, a proper content of TrFE is confirmed to be available to achieve a β-phase predominant P(VDF-TrFE).[34–36]

More recently, many researchers have realized that OPVDF shows more disadvantages and limitations compared to P(VDF-TrFE) for piezoelectric applications, including a lower decayed piezoelectric value at evaluated temperatures and a more natural shaping process.[37–42] However, some other scholars claimed that OPVDF possesses a very high ferroelectric to paraelectric temperature (F–P point or Currie point, T_c) above the melting point (>180 °C), while P(VDF-TrFE) films have a lower T_c.[22–26] They also believe that the low T_c value restricted their high temperature applications (*i.e.* aerospace and high energy vehicles). In fact, the T_c of P(VDF-TrFE) fully relies on the composition of VDF/TrFE, which means lower TrFE contents (20–30 mol%) in the copolymer can result in a higher T_c (above 100 °C).[32–34] It should be noted that the ferroelectric β phase of OPVDF is susceptible to temperature-induced stretching, which influences its piezoelectric properties greatly.[43] Thus, it is necessary to clarify the reason why the crystal structures of OPVDF become corrupted in addition to the deterioration of sample electrical performances with increasing temperature.

In this work, the domains, molecular chains, and the related conformations of OPVDF with different molecular weights under various polarizing processes were systematically investigated. Furthermore, we explored the reason why the domains of OPVDF cannot strictly be considered as a simple β crystal phase, like P(VDF-TrFE). OPVDF does not show the typical characteristics of a β-phase crystal domain but exhibits an activity akin to a matrix with all the aligned molecular chains in an all *trans* conformation, which further influences its related electric performances. Additionally, to provide an analysis of the practical application of P(VDF-TrFE) and OPVDF as a typical sensor, the differences between the two piezoelectric polymers in terms of their dielectric, ferroelectric, and piezoelectric properties were clarified. This enabled exploration of the polarizing process under the selected electric field. It is believed that the characterization of the electric properties, determining the relative mechanism analysis of their microstructure, as well as the sensor-capability detection of OPVDF and P(VDF-TrFE), will shed light on their practical applications in energy transfer devices.

2 Experimental

2.1 Preparation of PVDF and P(VDF-TrFE) films

PVDF powders with various molecular weights of 300k to 11 M and P(VDF-TrFE) with a TrFE molar content of 25% P(VDF-TrFE)75/25 were purchased from Solvay (USA) and Sigma Aldrich (USA), respectively. The polymer powders were dissolved in dimethylformamide (DMF) and further purified by filtering through a membrane. The polymer films had an average thickness of ~30 μm and were obtained by evaporating the solvent from spin-cast films at 100 °C for 6 hours. To obtain higher crystallinity, the films were heated to 200 °C for 6 hours followed by annealing at 140 °C for 6 hours. The obtained PVDF with molecular weights of 0.3 M, 0.5 M, 0.7 M, 0.9 M, and 1.1 M were marked as $PVDF_{0.3}$, $PVDF_{0.5}$, $PVDF_{0.7}$, $PVDF_{0.9}$, and $PVDF_{1.1}$, respectively. To fabricate the ferroelectric and piezoelectric properties of various PVDF films, the $PVDF_{0.3}$, $PVDF_{0.5}$, $PVDF_{0.7}$, $PVDF_{0.9}$, and $PVDF_{1.1}$ films were uniaxially oriented 5 times by a TA RSA-G2 dynamic thermo-mechanical analysis (DMA) instrument at a speed of 10 mm min^{-1} at 80 °C. The obtained samples were marked as $OPVDF_{0.3}$, $OPVDF_{0.5}$, $OPVDF_{0.7}$, $OPVDF_{0.9}$, and $OPVDF_{1.1}$, respectively.

2.2 Characterization

For electrical property characterization, by using an ion sputter coater (IXRF MSP-2S, Japan), a gold electrode with a diameter of 6 mm and a thickness of 80 nm was sputtered on both surfaces of the films. Differential scanning calorimeter (DSC, TA-Q2000) and X-ray diffraction spectrometers (XRD, RIGAKU D/MAX-2400, Rigaku Industrial Corporation, Japan) were utilized to characterize the crystal structures of the films. The wavelength of the X-ray was 1.542 Å (Cu Ka radiation, 40 kV, 100 mA, and 10° min^{-1}). The dielectric properties were detected using an Agilent (4294A and 4284) LCR meter with a temperature control system. The electric displacement–electric field loops (*D–E* loops) were obtained by a TF Analyzer 2000 ferroelectric test system, and an electric field with a triangular waveform at a frequency of 10 Hz was employed. To obtain high piezoelectric coefficients in the thickness direction (d_{33}), these films were polarized under a high electric field of 200 MV m^{-1} 10 times using the same ferroelectric test system. The acoustic signal from the sensor through charge-voltage conversion was measured and analyzed using an acoustic emission acquisition system (AMSY-6 Vallen System GmbH), where the response of a standard Pb-based lanthanum doped zirconate (PZT) acoustic emission sensor was used as a comparison.

3 Results and discussion

3.1 Configuration and conformation

Fig. 1 presents the ^{1}H NMR spectra and XRD diffraction patterns of five different molecular weight PVDF and P(VDF-TrFE) films. The assignment of ^{1}H NMR is as follows: the peaks at chemical shifts around 2.2 and 3.2 ppm are for VDF units with an H–H ($-CH_2CF_2-CF_2CH_2-$, H–H) sequence at 2.5–2.2 ppm (I_1), and at 3.2–2.8 ppm (I_2) for an H–T ($-CF_2CH_2-CF_2CH_2-$, H–T) sequence, respectively.[44] Thus, the molar composition of the PVDF can be calculated from eqn (1) and (2),

$$n_{H-H}\ (\text{mol\%}) = I_1/(I_1 + I_1) \quad (1)$$

$$n_{H-T}\ (\text{mol\%}) = I_2/(I_1 + I_2) \quad (2)$$

where, I_1 and I_2 refer to the integral of the peaks as assigned in the ^{1}H NMR spectrum, respectively. The ratio of the number of H–H (or T–T): H–T in PVDF of different molecular weights was calculated as follows: $PVDF_{1.1}$: $n_{H-T} : n_{H-H} = 11 : 1$, $PVDF_{0.9}$:

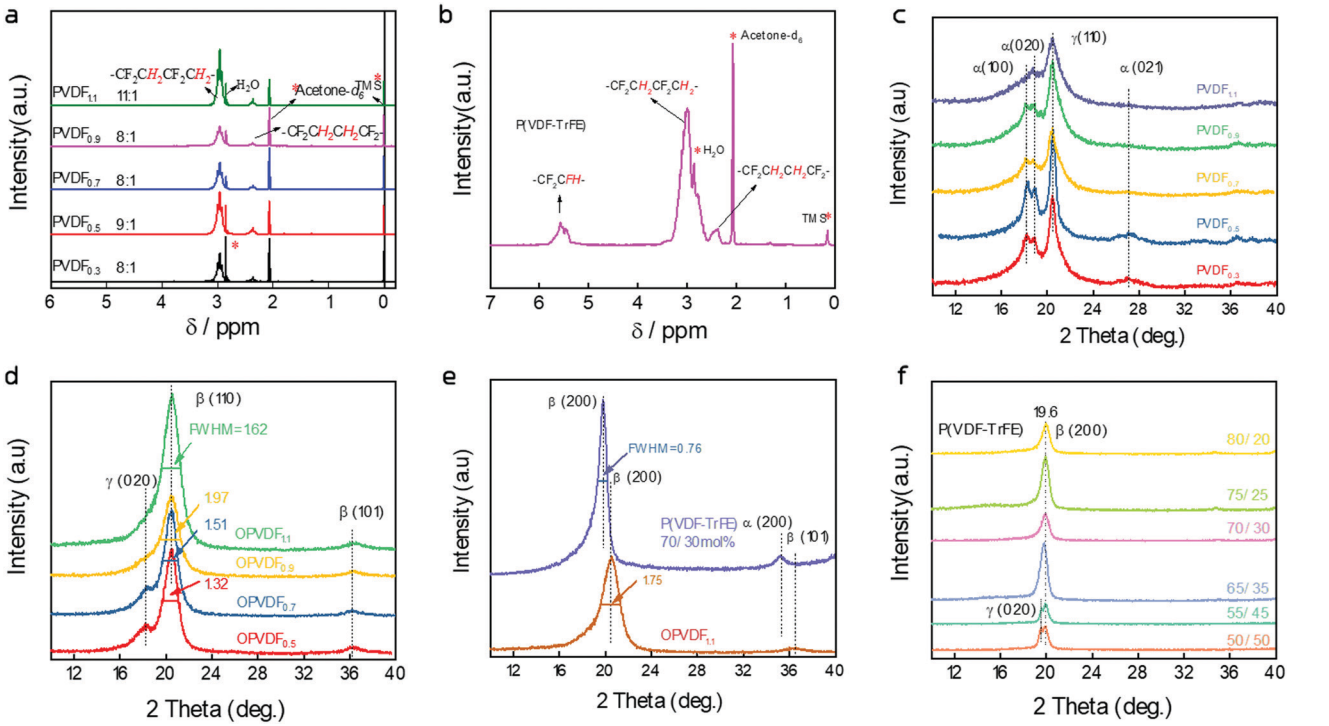

Fig. 1 ^{1}H NMR spectra and XRD diffraction patterns of five different molecular weight PVDF and P(VDF-TrFE) films. (a) PVDF with different molecular weights, (b) P(VDF-TrFE)75/25 mol%, (c) un-treated PVDFs, (d) oriented PVDFs, (e) P(VDF-TrFE) 70/30 mol% film and oriented PVDF, and (f) various P(VDF-TrFE) films. The full width at half maximum (FWHM) of the (110) and (200) peaks are labeled.

n_{H-T}:n_{H-H} = 8:1, $PVDF_{0.7}$: n_{H-T}:n_{H-H} = 8:1, $PVDF_{0.5}$: n_{H-T}:n_{H-H} = 9:1, and $PVDF_{0.3}$: n_{H-T}:n_{H-H} = 8:1. This closed ratio of H–H and H–T in different PVDF samples had a slight effect on their electrical properties. Comparatively, in the ^{1}H NMR results for P(VDF-TrFE), there appears to be a shoulder peak of 5.3–5.7 ppm, which refers to a TrFE unit, as shown in Fig. 1(b), and the peaks of 3.2–2.8 ppm refer to the H–T sequence of VDF. Moreover, the weak peak at 2.5–2.2 ppm indicates that the VDF monomer in P(VDF-TrFE)75/25 is mostly connected in a H–T conformation, which favors high electric polarization.

Besides the investigation on the monomer connection for the polymerization of VDF or TrFE, it is also important to study the crystal phase dependence of the molecular structure of OPVDF and P(VDFTrFE). The XRD patterns of various samples are presented in Fig. 1(c)–(f). Fig. 1(c) shows the phase structures of un-treated PVDF with their split diffraction peaks ranging from 18° to 21°. $PVDF_{0.5}$ corresponds to mainly an α phase. $PVDF_{0.7}$ and $PVDF_{0.9}$ have coexisting α and γ phases. Comparatively, $PVDF_{1.1}$ is γ phase predominant, according to the two peaks at 18.5° and 20.1° (planes 020 and 110).[45] After mechanical orientation, $OPVDF_{0.5}$, $OPVDF_{0.7}$, $OPVDF_{0.9}$, and $OPVDF_{1.1}$ all have a very high single peak at ~20.8°, which refers to the (200) plane and corresponds to the β phase area.[46]

In all the OPVDF films, the diffraction peak around 20° has already been expressed as symbolic of the all *trans* phase, as depicted in Fig. 1(d). In most of the academic research and engineering applications, the OPVDF shows the characteristics of ferroelectrics possessing spontaneous polarity. This study does not completely contradict this statement of OPVDF as ferroelectrics. However, it is reasonable to believe that the crystal region of OPVDF does not actually possess the nature or whole β phase grains like P(VDF-TrFE) but consists of an alignment of ordered VDF molecular chains, as shown in Fig. 2(c). Thus, the XRD patterns of P(VDF-TrFE) films with various TrFE contents are different from that of OPVDF, as compared in Fig. 1(d)–(f) where the main peak of P(VDF-TrFE) is located at below 20° and all OPVDFs at above 20°. In addition, the content of TrFE has little influence on the location of the diffraction peaks in different P(VDF-TrFE) films. As shown in Fig. 1(f), the patterns of most P(VDF-TrFE) films have a sharp peak at 19.6°, corresponding to the (200) plane and are the classic response of the β phase.[1,23,46] Besides, a weak peak of 20.24° (plane 110) in the presence of the γ phase is suggested to be present in P(VDF-TrFE)55/45 mol% and 50/50 mol% since the higher content of TrFE acts as a block and breaks the sequences of the β phase molecular chains.[47–49] The main diffraction peaks at 19.6° in P(VDF-TrFE)65/35 mol% and P(VDF-TrFE)75/25 mol% are higher than other P(VDF-TrFE) films, indicating that these two samples possess a higher crystallinity. The P(VDF-TrFE)55/45 mol% and P(VDF-TrFE)50/50 mol% films consist of smaller crystal lamellar grains than other P(VDF-TrFE) samples. In addition, we present the full width at half maximum (FWHM) of the (110) peaks and (200) peaks in Fig. 1(d) and (e), respectively. The narrower FWHM results in a smaller size of crystal structures, which has been previously proved in the literature.[50] Thus, as compared in Fig. 1(e), the FWHM of 0.76 in the P(VDF-TrFE)70/30 mol% film is far narrower than that of $OPVDF_{1.1}$

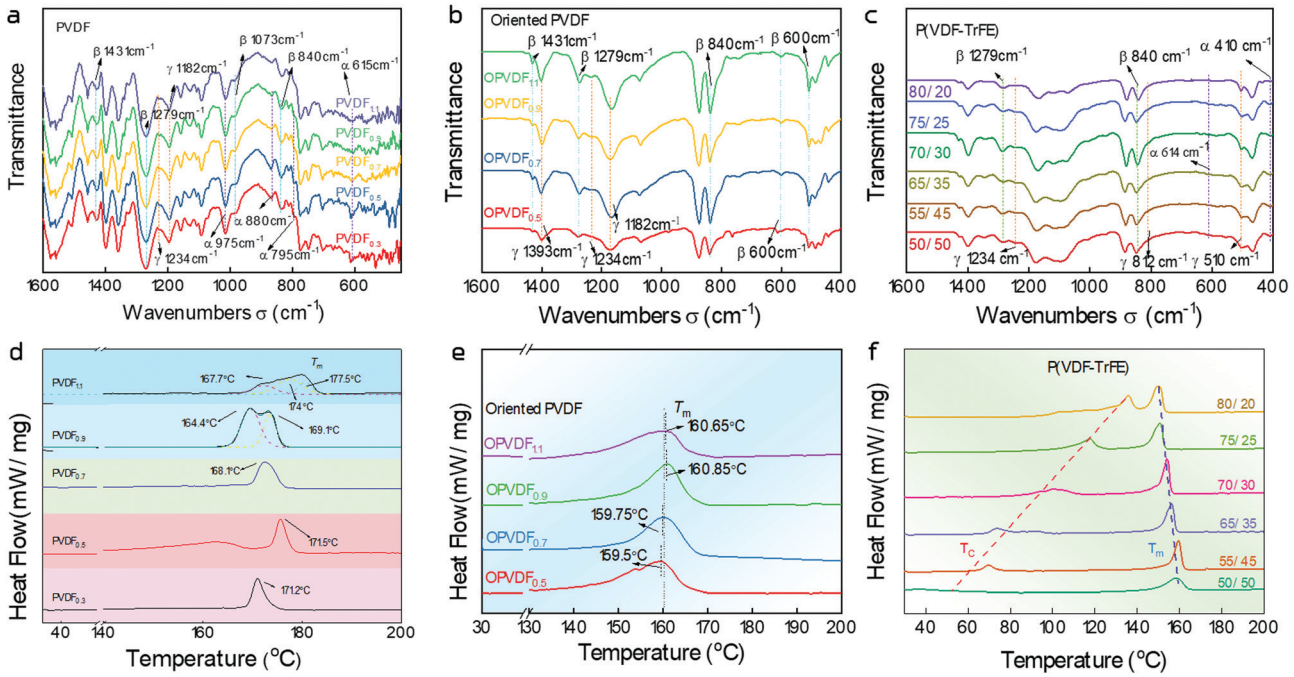

Fig. 2 FTIR spectra and DSC curves of PVDF and P(VDF-TrFE): (a) FTIR of PVDF films with different molar weights, (b) FTIR of OPVDF films with varying molar weights, (c) different P(VDF-TrFE) films, (d) DSC curves of PVDF films with varying molar weights, (e) DSC curves of PVDF films with different molar weights and (e) different P(VDF-TrFE) films.

of 1.75, illustrating that this copolymer possesses a more perfect crystal size and crystal area than the oriented PVDF.

To further assess the different alignments of all *trans* molecular chains in P(VDF-TrFE) and OPVDF, the chain conformations and crystal phases are compared by analysing the FTIR and DSC results, as presented in Fig. 2. The characteristic absorption peaks at 615 cm^{-1}, 795 cm^{-1}, 880 cm^{-1}, and 976 cm^{-1} can determine the α phase of VDF, the peaks of 840 cm^{-1}, 1880 cm^{-1}, 1073 cm^{-1}, 1279 cm^{-1}, and 1431 cm^{-1} refer to the β conformation of PVDF, and the absorption peaks at 1182 cm^{-1} and 1234 cm^{-1} correspond to the γ conformation.[51,52] As shown in Fig. 2(a), the absorption bands of various PVDF samples indicate that this unstretched polymer is a mixture of phases, including α (761, 795, 975, 1146, 1209, and 1380 cm^{-1}), γ (843 and 1240 cm^{-1}), and a low content of β phase (843 and 1276 cm^{-1}). The absorption bands for the γ/β phases are quite weak, which indicates that the unstretched PVDF is α phase dominated. The small amounts of γ/β phases could be a result of homogeneous nucleation/fast crystallization when the samples are quenched by an ice water mixture. However, the β and γ phases in FTIR are difficult to identify because the two phases have similar polymer chain conformations and close characteristic absorption bands at 510 cm^{-1}, 810–840 cm^{-1}, and 1284–1290 cm^{-1}. In addition, the FTIR results in Fig. 2(b) indicate that the β and γ conformations coexist in OPVDF. The intensity of the absorption peaks of the β phase at 840 cm^{-1}, 1279 cm^{-1} and 1413 cm^{-1} slightly increase with the increase of molecular weight which indicates that OPVDF with a higher molar weight has a longer molecular chain than that of samples with low molar weights and thereby possesses a larger β-phase aligned region. Meanwhile, Fig. 2(c) shows that all P(VDF-TrFE) is β-phase predominant for the absorption peaks at 840 cm^{-1}, 1279 cm^{-1}, and 1413 cm^{-1}.

The DSC curves, as shown in Fig. 2(d)–(f), further prove the differences in crystal structures of stretched PVDF and P(VDF-TrFE) films. Before orientation, $PVDF_{0.5}$ and $PVDF_{0.7}$ samples contain a single phase transformation at ~170 °C, corresponding to the T_m of the α phase. Comparatively, $PVDF_{0.9}$ has two different heat flow peaks at 164.4 °C and 169 °C, corresponding to the α and γ phases, respectively, using the DSC peak-differentiating and imitating technology mentioned in the literature.[38] The three peaks of $PVDF_{1.1}$ at 167.7 °C, 174 °C, and 177.5 °C refer to a multi-phase of α + γ + β. After five-time stretching, the DSC curves of all OPVDF only have a single T_m peak at ~157 °C, which refers to a single phase of the aligned all *trans* molecular chains.

The heat flow changes of P(VDF-TrFE) are very different from OPVDF films, as shown in Fig. 2(e). The P(VDF-TrFE) film has two intensified peaks which confirm that the low peak is T_c of the β crystal phase, and the high one is the T_m of the P(VDF-TrFE) film. All OPVDF films do not show a definite T_c. Meanwhile, the intensities of T_c or T_m of P(VDF-TrFE) are higher than the T_m of OPVDF as shown in Fig. 2(f). One reason for this is that P(VDF-TrFE) possesses large and structured crystal grains of the β phase, while P(VDF-TrFE) has compact crystal regions, and OPVDF shows only the crystalline region which can be attributed to long-range order of straight molecular chains.

3.2 Electrical polarization and dielectric properties

Based on the detailed analysis of configuration and conformation, unstretched PVDF possesses an α-predominated crystal phase, which shows the characteristics of relaxed ferroelectricity,

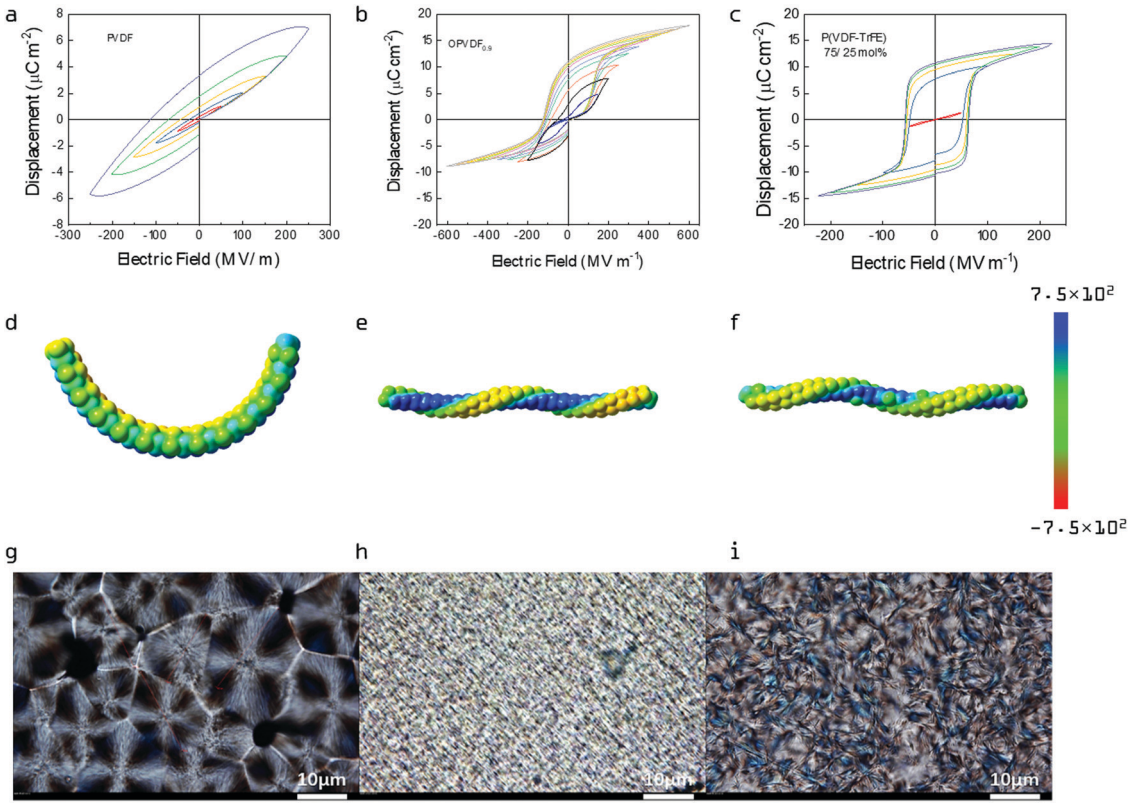

Fig. 3 *D–E* hysteresis loops, molecular potential simulation, and POM graphics of OPVDF and P(VDF-TrFE). (a–c) *D–E* loops of the $PVDF_{0.9}$, $OPVDF_{0.9}$, and P(VDF-TrFE)75/25% films. (d–f) The molecular potential simulation of the $PVDF_{0.9}$, $OPVDF_{0.9}$, and P(VDF-TrFE)75/25 mol% films. (g) and (h) POM graphics of the *D–E* loops of the $dPVDF_{0.9}$, $OPVDF_{0.9}$, and P(VDF-TrFE)75/25% films.

as shown in Fig. 3(a). After orientation, OPVDF possesses well-aligned all *trans* molecular chains rather than regular β-phase crystal grains. It is considered that dipoles in the all *trans* molecular chains of OPVDF polarize more easily along with the electric field than the β-phase crystal grains, and OPVDF does not contain a $–CF_2–CFH–$ segment to reduce the polarity of dipoles as in P(VDF-TrFE). Therefore, OPVDF should exhibit a more significant electric displacement than P(VDF-TrFE) under the same electric field and one at least equal to P(VDF-TrFE).

However, the displacement *vs* electric field (*D–E*) loops shown Fig. 3(b) indicate that the maximum and remnant electric displacement (P_m and P_r) of OPVDF are smaller than that of P(VDF-TrFE). And in particular, P_m of OPVDF increases progressively with the electric field and saturation is not reached, even up to 600 MV m^{-1}. This indicates that there are still increasing dipoles in the OPVDF response which enhances the electric field continuously. This trend is different from the *D–E* loops of P(VDF-TrFE) whose P_m reaches saturation under 250 MV m^{-1}, as illustrated in Fig. 3(c). Moreover, the coercive electric field (E_c) of OPVDF is ~100 MV m^{-1} which is larger than that of P(VDF-TrFE) (~50 MV m^{-1}), indicating that the dipoles and crystal domains in OPVDF are more difficult to reverse than that of P(VDF-TrFE).

Why do OPVDF and P(VDF-TrFE) have these apparent differences as a result of the polarization process? It was thought that this could be attributed to the VDF molecular chain alignment in different films and therefore Fig. 3(d)–(f) provided the simulated results of electrostatic potential using the Accelrys software, where the cool tone (blue and dark green) and warm tone (red and orange) represent the positive and negative charge distribution, respectively. Clearly, the molecular chain of PVDF looks like a bow where the positive and negative charges distribute along the side of the backbone, and there are no apparent all-*trans* dipoles. Comparatively, OPVDF and P(VDF-TrFE) molecular chains show a helical charge distribution. The reason for this is that although OPVDF is mechanically oriented, it shows a static potential stable state. As for P(VDF-TrFE), for the insertion of the TrFE wedge, the static charges are forced to distribute in different directions of the molecular chains of P(VDF-TrFE), and therefore, the molecular chains of P(VDF-TrFE) develop a higher electric dipole moment. Nevertheless, from the fitting results of the static potential distribution, the configuration of P(VDF-TrFE) is not superior to that of OPVDF in terms of contribution to electrical polarization.

To explain the preferable ferroelectric properties of P(VDF-TrFE), Lei Zhu's group have expressed the various *D–E* loops of PVDF-based co- (ter-) polymers from the diversities of the inter-chain distance and dipole moment, and they propose that the changes in the *D–E* loops are caused by the introduction of other monomers (CTFE, TrFE, and CFE) or e-beamed irradiation.[38] However, the relatively low polarization in the *D–E* loops of OPVDF can exclude the influence of supplemental monomers and thereby the differences in conformation, including molecular

chain structures, ferroelectric domain, or even crystal grain, may result in the diversity.

Therefore, it is believed that two critical factors cause this phenomenon: (1) the reversal of the ferroelectric domains, consisting of dipoles $-CF_2-CH_2-$ in OPVDF, may suffer from a higher resistance of the van der Waals forces of the neighboring molecular chains or domains, and (2) dipoles of the $-CF_2-CH_2-$ chains in OPVDF are not aligned in the same plane or connected with a helical structure, resulting in many $-CF_2-CH_2-$ dipoles linked in different directions which reduce the polarity of the whole molecular chain. To clarify the crystalline dependencies of the ferroelectric and dielectric properties of the OPVDF and P(VDF-TrFE) films, the crystal grains of unstretched PVDF, OPVDF and P(VDF-TrFE) films were studied. Clearly, $PVDF_{0.9}$ possesses large α crystalline grains, and as expected $OPVDF_{0.9}$ shows no crystal grain, as shown in Fig. 3(g) and (h). The crystal region of $OPVDF_{0.9}$ can be highlighted as a region that shows characteristics of the β phase. The XRD patterns in Fig. 1(e) had proved the differences in the crystalline properties of OPVDF and P(VDF-TrFE). Therefore, the crystalline region of $OPVDF_{0.9}$ can be considered as an aligned β phase of nano-crystal slices. The crystalline region of P(VDF-TrFE) shown in Fig. 3(i) readily forms a perfect β phase crystal lamella.

In actual fact, the spherocrystal grains in PVDF consist of numerous crystal plates, which include many aligned folded molecular chains of α or γ. The α-phase spherocrystal grain is without polarity, while the γ-phase one has a weak polarity. Therefore, the dipoles in the crystal region have almost no contribution to P_m under a high electric field. After mechanical orientation, almost all the molecular chains in the spherocrystal grains and amorphous regions are straightened along the in-plane direction of the OPVDF films. Simultaneously, the molecular chains of PVDF convert from a thermostable state of α or γ to the strain-induced all *trans* phase.

Meanwhile, the crystal domains consisting of all *trans* molecular chains are randomly distributed in the out-of-plane direction of the film, which can be increasingly poled and reversed gradually with an increase in the electric field. However, the ferroelectric domain of the OPVDF film consists of the straightened molecular chains rather than the overlapping ones of $-CH_2-CF_2-$, which needs a higher electric strength to be poled. Therefore, the *D*–*E* loops of OPVDF show a higher E_c than that of P(VDF-TrFE). Moreover, the P_m of $OPVDF_{1.1}$ increases with the increasing electric field due to the continued polarization of the randomly distributed domains, as shown in Fig. 3(b). Comparatively, P(VDF-TrFE) has relatively small crystal domains with large amorphous regions consisting of chaotic molecular chains that have little restraint to the movement of the crystal domains. As such, the crystal domain of P(VDF-TrFE) can respond to low electric fields, resulting in a lower E_c and P_m than that of OPVDF under the same electric field, as shown in Fig. 3(b) and (c).

As depicted above, in the orientation process, PVDF is subject to a phase transition, which will influence the dielectric properties. Fig. 4 compares the dielectric properties of unstretched PVDF and OPVDF films with various molecular weights. Before orientation, $PVDF_{1.1}$ shows a dielectric constant of 11 which is larger than that of the $PVDF_{0.5–0.9}$ films. This is due to $PVDF_{1.1}$ possessing a mixture of α + γ + β phases and a β phase region that was well proved to have a higher dielectric response than the other two phases of α and γ. Therefore, $PVDF_{0.5}$ consisting of almost a nonpolar α phase shows a low dielectric constant of 8.5, as shown in Fig. 4(a). After being stretched 5 times,

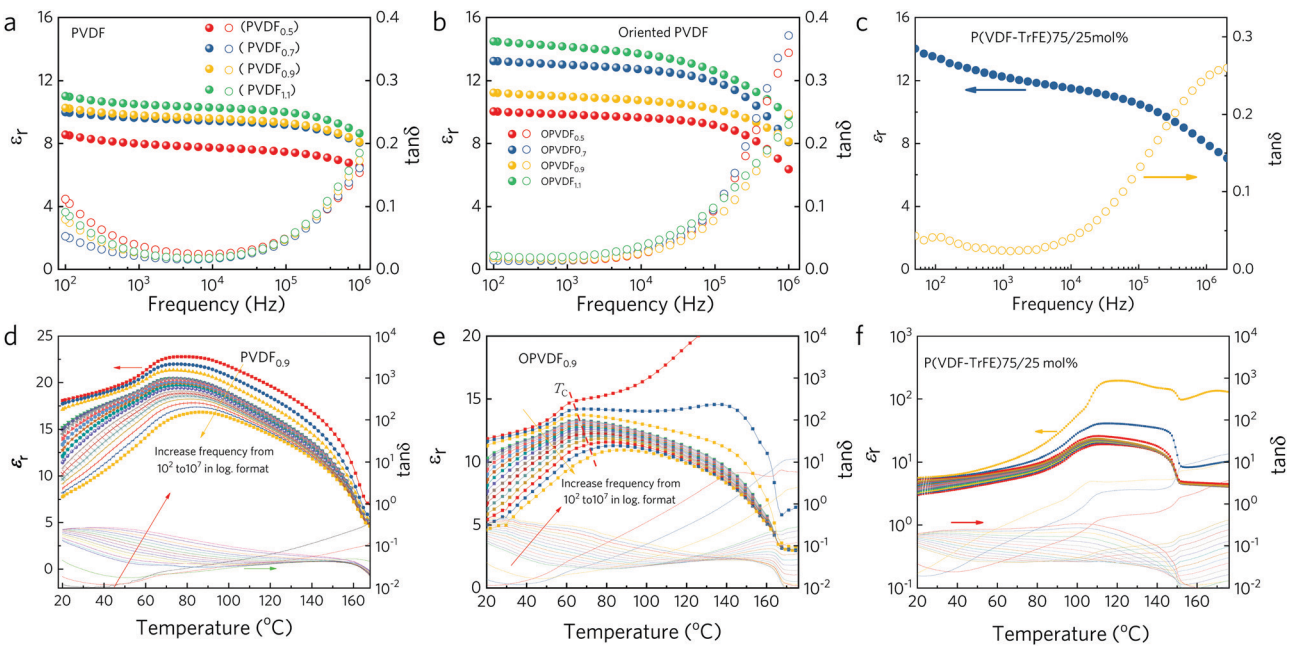

Fig. 4 Dielectric properties of PVDF films with different molecular weights. (a) Un-stretching PVDF films, (b) OPVDF films, (c) P(VDF-TrFE)70/30 mol%, (d) dielectric properties vs temperature of $PVDF_{0.9}$, (e) dielectric properties vs temperature of $OPVDF_{0.9}$, and (f) dielectric properties vs temperature of P(VDF-TrFE)70/30 mol%.

most of the α and γ phases in PVDF converted into a β phase-like long-range order region, which favors a high dielectric response and therefore, the dielectric constant of all the OPVDF films increased, and $OPVDF_{1.1}$ showed a relatively large dielectric constant (ε_r) of 14.5 due to its highly aligned all *trans* dipoles, as illustrated in Fig. 4(b). Similarly, Fig. 4(c) demonstrates that the introduction of TrFE shows no obvious influences on the dielectric properties of P(VDF-TrFE)70/30 mol%.

In addition, the comparison of the dielectric loss ($\tan\delta$) of the unstretched PVDF and OPVDF films can illustrate the phase transition behavior of these films, as presented in Fig. 4(a)–(c). At low frequencies, unstretched PVDF films show a larger $\tan\delta$ than OPVDF. The reason for this is that unstretched PVDF includes more defects and impurity ions caused by the fabrication process, resulting in interfacial polarization, which correlates to the low frequency (<1 kHz) response. In contrast, the interfacial polarization in OPVDF is significantly reduced, and thereby, $\tan\delta$ at a low frequency is depressed. However, $\tan\delta$ of OPVDF at high frequencies is more significant than the unstretched samples because of the increment of the aligned molecular chains. The dipole reversal in these crystalline-like regions may suffer from being more restricted than in the amorphous regions of unstretched PVDF. Therefore, $\tan\delta$ of $OPVDF_{0.9}$ and $OPVDF_{1.1}$ increased to about 0.35 at a high frequency of 1 MHz.

Fig. 4(d)–(f) show the dielectric broadband spectra of $PVDF_{0.9}$, $OPVDF_{0.9}$ and P(VDF-TrFE)75/25 mol% films at a wide temperature range from −60 to 120 °C. At high temperatures above 80 °C, the ε_r of $OPVDF_{0.9}$ and P(VDF-TrFE) is more significant than at low temperatures. Since a perfect β crystal grain has not formed, $OPVDF_{0.9}$ has no apparent T_c point, as shown in the DSC curves in Fig. 3(c). Conversely, P(VDF-TrFE) shows a clear T_c point. Therefore, the ε_r of $OPVDF_{0.9}$ shows a tiny increment at a high temperature while the ε_r of P(VDF-TrFE)75/25 mol% has a dramatic enhancement at 80–100 °C and even reaches 1 k at 10 Hz. Simultaneously, $\tan\delta$ of P(VDF-TrFE) at 80–120 °C in the low-frequency region (0.1–10 kHz) abnormally increases due to the relaxation of ferroelectric dipoles around the T_c point. Comparatively, at a low temperature from −60 °C to 40 °C below T_c, $\tan\delta$ is relatively stable at various frequencies. These comparisons on dielectric broadband spectra further indicate that the F–P transition behavior of the β crystal phase in the $OPVDF_{0.9}$ sample is weaker than the standard ferroelectric copolymer P(VDF-TrFE).

As discussed above, it seems that OPVDFs cannot be considered as typical ferroelectrics. However, over the past few decades, commercially available OPVDF films have exhibited a proper piezoelectric performance and been shown to have great prospects for applications.

What happens in pure PVDF films from raw materials to piezoelectric OPVDF films in the electrical polarization process? To clarify the reversal of dipoles in OPVDF, Fig. 5 compares the *D*–*E* loops of unstretched PVDF and OPVDF under various electric fields. As shown in Fig. 5(a), the *D*–*E* loops of all unstretched PVDF films with different molar weights show a spindly loop under a high electric field of 200 MV m^{-1}. This indicates that untreated PVDF films are relaxor ferroelectrics since these PVDF films are α-phase predominate, which has been illustrated by XRD and DSC results.

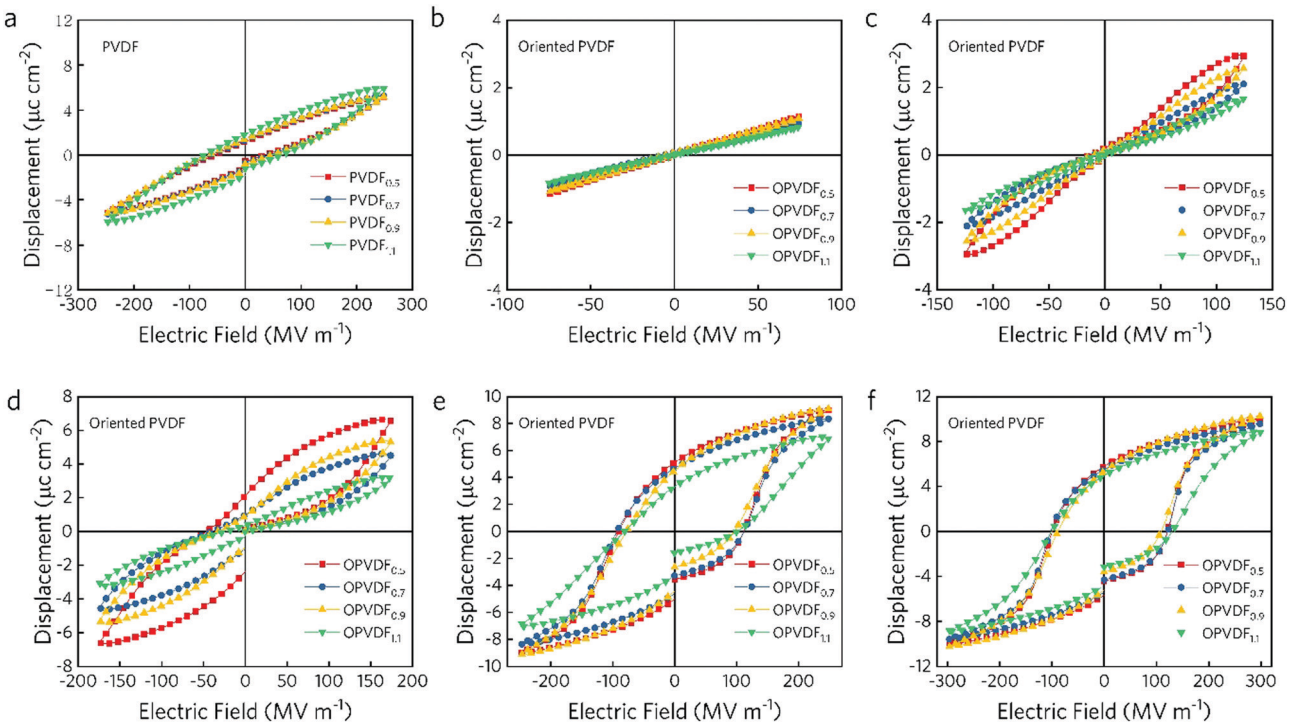

Fig. 5 *D*–*E* hysteresis loops of PVDF under different electric fields: (a) 250 MV m^{-1}, (b) 75 MV m^{-1}, (c) 125 MV m^{-1}, (d) 175 MV m^{-1}, (e) 275 MV m^{-1}, and (f) 300 MV m^{-1} films.

However, the OPVDF films show a different polarizing process, as shown in Fig. 5(b)–(f). Clearly, under 75 MV m^{-1} the *D–E* loops of all OPVDF films are almost linear-shaped, which is attributed to the vibration of molecular chains, electronic, atom polarizations, *etc.* from the amorphous regions, and the dipoles have not been able to respond to the low electric field of 75 MV m^{-1}. Moreover, $OPVDF_{0.5}$ and $OPVDF_{0.7}$ samples show a larger P_m than $OPVDF_{1.1}$ and $OPVDF_{0.9}$. The reason for this is that OPVDF with a low molar weight possesses a lower and smaller all *trans* aligned β region, which is able to respond to the low electric field. It is the more amorphous $OPVDF_{0.5}$ and $OPVDF_{0.7}$ samples that contribute to the displacement under 75 MV m^{-1} early, as illustrated in Fig. 5(b).

With the electric field increased to 125 MV m^{-1}, the all *trans* dipoles in OPVDF start to reverse and respond to the electric field, and it appears that the *D–E* loops in Fig. 5(c) have a shape change from lined to a narrow double hysteresis loop (DHL). As such, for possessing smaller all *trans* aligned β regions, $OPVDF_{0.5}$ begins the transition from linear dielectric to antiferroelectrics. Subsequently, $OPVDF_{0.7}$, $OPVDF_{0.9}$, and $OPVDF_{1.1}$ have a similar transition at 175 MV m^{-1}, as shown in Fig. 5(d). Up to 250 MV m^{-1}, the P_r of all the OPVDF films shown in Fig. 5(e) increases dramatically, indicating that the considerable ferroelectric domains in these samples are reoriented along the direction of the electric field. When the electric strength further increases to 300 MV m^{-1}, the P_m and P_r of $OPVDF_{0.9}$ reach the high values of 10 μC cm^{-2} and 7 μC cm^{-2}, respectively, as illustrated in Fig. 5(f). Fig. 5(f) also shows that the E_c of all OPVDF films is about 100 MV m^{-1} due to a slow response of large blocks of all *trans* aligned β regions, *i.e.* the dipoles in OPVDF start to respond to electric fields above 100 MV m^{-1}. With the increase in electric field from 125 MV m^{-1} to 300 MV m^{-1}, the all *trans* dipole reversal continuously responds to the poling strength and the P_m and P_r of OPVDF increase accordingly. However, there is still a large proportion of dipoles without polarization, even when the electric field reaches 300 MV m^{-1}, and the *D–E* loops of OPVDF films cannot reach saturation. On the other hand, whether the poled dipoles which have been reversed can remain stable is still a question that should be further discussed. These dipoles in the OPVDF films incur a forced orientation through mechanical stretching and electrical polarization, which is thermodynamically unstable and easy to disorder.

3.3 Piezoelectric properties

To investigate the stability of the piezoelectric properties of OPVDF and P(VDF-TrFE), Fig. 6(a) compares the changes of the piezoelectric properties of these films with increasing temperature. d_{33} of the OPVDF films linearly decreases with increasing temperature when the temperature increases from 25 to 130 °C, and d_{33} decreases from −17.0 pC N^{-1} to −6.47 pC N^{-1}. Attractively, the d_{33} of the P(VDF-TrFE)75/25 mol% film remains at a high level of above −20 pC N^{-1} under a wide temperature scale from 20 to 110 °C, and after 115 °C it sharply decreases from −21.5 pC N^{-1} to −5.55 pC N^{-1}. Moreover, Fig. 6(b) compares the electromechanical performance of the two samples. Both OPVDF and P(VDF-TrFE)75/25 mol% films show resistance to the resonance phenomenon at a frequency range of 30–50 MHz. By using the fitting method reported in the recent literature,[39,53,54] the electromechanical coupling coefficient (k_t) was obtained in the thickness model of OPVDF (k_t = 0.26) and P(VDF-TrFE)75/25 mol% (k_t = 0.30), indicating that the P(VDF-TrFE) piezoelectric film has a higher electromechanical conversion efficiency than OPVDF.

For OPVDF samples, the all *trans* molecular chains are shown with an artificial orientation in Fig. 6(a). This decreasing d_{33} may be explained macroscopically by the movement of the oriented molecular chains, where the high temperature can improve the free volume and mobility of the oriented chain segments and provide more significant space for the orientation of grains along the electric field. Also, the entropy of the all *trans* structured molecular chains in OPVDF has the maximum value, which corresponds to the thermodynamically unstable state. With the temperature increase, the intermolecular segments will be oriented more freely and tend to be continuously disordered, leading to a decrease of d_{33}.

Comparatively, molecular chains in the β-phase of P(VDF-TrFE) are involved in a large crystal grain. Although the VDF and TrFE molecular chains are also a thermodynamically unstable alignment, the inserted block monomer TrFE can restrain the disordered VDF or TrFE fractions and let them remain in a

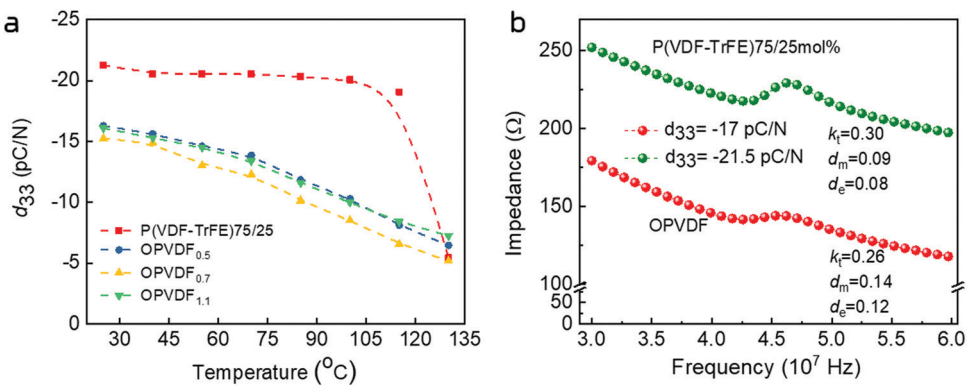

Fig. 6 Piezoelectric constant and electromechanical coupling performance fitting of the OPVDF and P(VDF-TrFE) films. (a) The recession of the piezoelectric constant with the increasing temperature. (b) Impendence *vs.* frequency and fitting of electromechanical coupling performance.

relatively stable state until the molecular chains are given sufficient thermal energy at T_c. That is to say, the spontaneous polarization in OPVDF results from the ordered β phase molecular chains in the whole membrane region. Otherwise, the polarity of P(VDF-TrFE) is contributed by the separated crystal grains composed of molecular chain-folded lamellae. This is the reason why P(VDF-TrFE) can withstand the influence of a higher temperature on the disordered activity of molecular chains than OPVDF.

3.4 Acoustic emission reception

To investigate the acoustic emission (AE) reception property of a P(VDF-TrFE) piezoelectric film that has been polarized and has a d_{33} of −21.5 pC N^{-1}, a piece of 0.5 mm pencil lead was broken on a plexiglass plate to simulate a Nielsen–Hsu acoustic emission source.[38] This is the most commonly used simulated acoustic emission source in emission detection technology. Fig. 7(a) and (b) present the AE test system and a scheme of the transmitting procedure of a lead-break signal. As shown in Fig. 7(b), a preamplifier with a gain of 34 dB has been connected to the sensor, where the ratio in decibel (or dB) is calculated as eqn (3) in a logarithmic scale.

$$A\ [\mathrm{dB}] = 20 \times \log(U_{\max}/1\ \mu\mathrm{V}) \quad (3)$$

where, A characterizes the relative ratio of wave energy in dB, and $U_{\max}$ is the peak amplitude of stress wave signals. For instance,

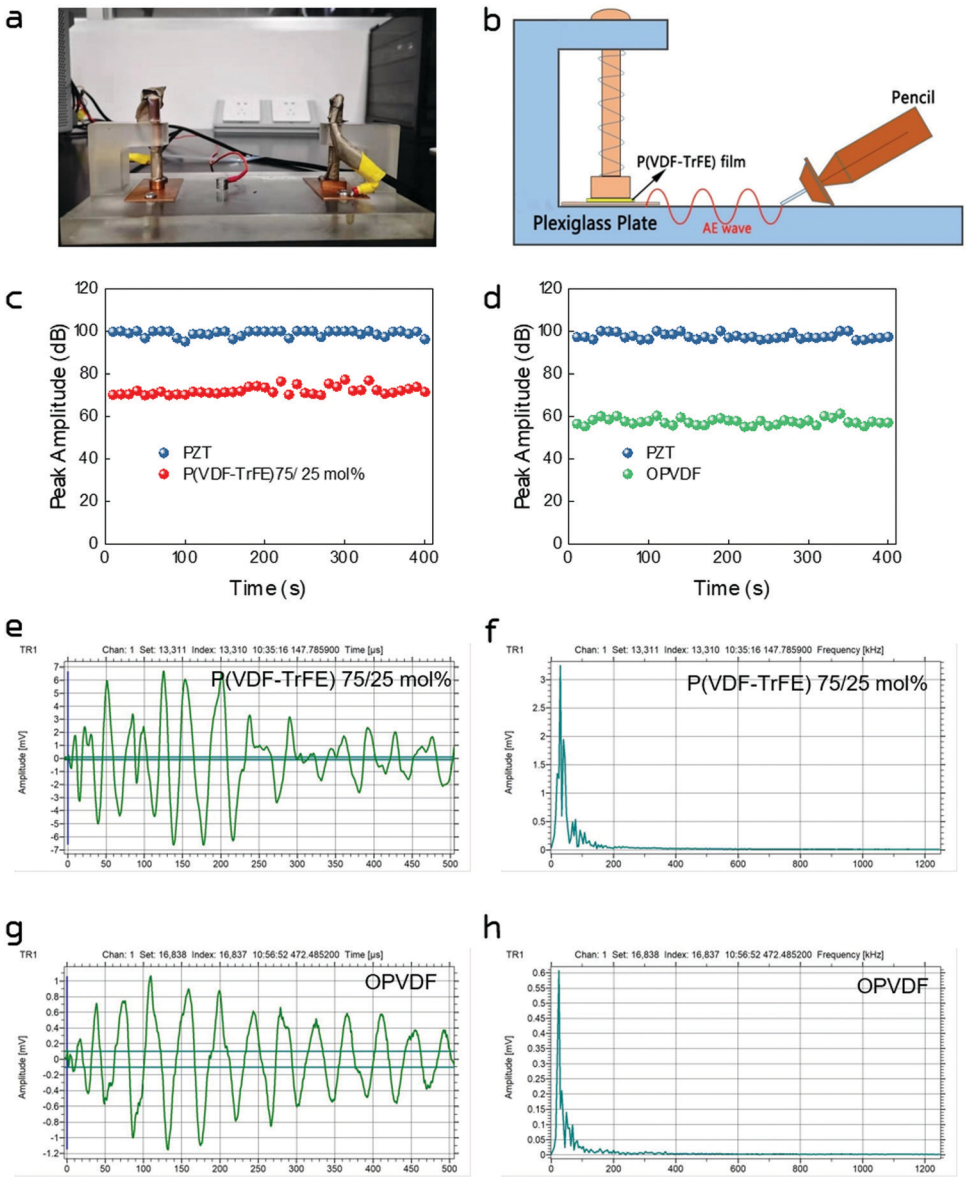

Fig. 7 Acoustic emission reception property of P(VDF-TrFE) and OPVDF films, and a commercial PZT is used for comparison: (a) test devices, (b) scheme of an acoustic emission reception test, (c) peak amplitude of P(VDF-TrFE)75/25 mol%, (d) peak amplitude of the OPVDF film, (e and f) represent the time-amplitude correlation diagrams of P(VDF-TrFE)75/25 mol% and OPVDF, and (g and h) are the frequency-amplitude correlation diagrams of P(VDF-TrFE)75/25 mol% and OPVDF, respectively.

if the gain is 34 dB, the amplitude of the AE signal from the sensor is amplified by a factor of 50. The time-amplitude correlation diagram and waveform diagram received by the sensor are presented in Fig. 7(c) and (d). A commercial PZT is used as the reference and the corresponding peak amplitudes are around 100 dB. For its perfect piezoelectric performance, most of the peak amplitudes of P(VDF-TrFE) are distributed around 70 dB, which is higher than that of OPVDF (56 dB). Moreover, the time-magnitude correlation graph in Fig. 7(e) and (g) shows that P(VDF-TrFE) has a signal response of 6 mV at 0–300 μs, whose magnitude is more significant than that of OPVDF ($\sim$1 mV). The frequency-magnitude correlation graph in Fig. 7(f) and (h) also shows that P(VDF-TrFE) and OPVDF have a wide response frequency range of 10–100 kHz, and P(VDF-TrFE) possesses a high maximum signal output of 3.2 mV. Therefore, the acoustic emission performance of P(VDF-TrFE)75/25 mol% films with an amplitude of about 70 dB is superior to the commercial OPVDF sensor, which is a potential coordinate for acoustic emission sensors in flexible electronic devices.

4 Conclusions

In summary, the crystal property dependence of the dielectric and ferroelectric performances of pure PVDF films with various molecular weights and P(VDF-TrFE) films were investigated. It was found that the crystal regions of unstretched PVDF consist of α, β and γ mixed crystal phases. After orientation, the OPVDF films changed from a nonpolar α to polar β phase. However, the phase transformation of OPVDF is very different from P(VDF-TrFE), which is just the whole alignment of all *trans* PVDF molecular chains. Additionally, P(VDF-TrFE) has a relatively perfect molecular chain-folded lamellae. Consequently, the main diffraction peak of oriented PVDF and P(VDF-TrFE) is slightly different. The DSC and dielectric temperature spectra indicate that an oriented PVDF is not a typical ferroelectric because it does not show a clear transition point from a ferroelectric to paraelectric phase. Moreover, the ordered β phase molecular chains in the whole membrane region are easily disordered with an increment in temperature, and the piezoelectric coefficient of oriented PVDF is lower than that of P(VDF-TrFE), and it starts to decrease from a low temperature of 40 °C. Comparatively, the normal ferroelectric characteristics of P(VDF-TrFE) are confirmed by hysteresis loops and, more interestingly, it possesses a temperature-independent piezoelectric coefficient of -21.5 pC N^{-1} below 120 °C. Additionally, the P(VDF-TrFE) piezoelectric film sensors respond best to the signal with an amplitude of about 70 dB, which is equivalent to the traditional PZT sensor. The more reliable piezoelectric, electromechanical coupling effect and acoustic emission reception performance of P(VDF-TrFE) is valuable for a flexible and thermally stable piezoelectric film replacing oriented PVDF or even ceramic piezoelectrics.

Author contributions

W. X. and L. Z. supervised the work. Z. Z. and J. L. prepared the samples, performed the measurements, and wrote the manuscript. C. C. worked on the simulations. X. Z and T. S. analyzed the acoustic performance. All authors have given approval to the final version of the manuscript.

Conflicts of interest

The authors declare no competing financial interests.

Acknowledgements

This work was supported by the National Nature Science Foundation of China-NSAF under grants 51773168, 51802182, and 51972263, and the 111 Program (No. B14040). Jinglei Li thanks the Fundamental Research Funds for the Central Universities (Grant No. sxjh012019011).

References

1 R. G. Kepler and R. A. Anderson, Ferroelectric polymers, *Adv. Phys.*, 1992, **41**, 1–57.
2 H. S. Nalwa, *Ferroelectric Polymers-Chemistry, Physics and Applications*, Marcel Dekker Inc., New York, 1995, p. 203.
3 J. M. Herbert; A. M. Glass and T. T. Wang, *The Application of Ferroelectric Polymers*, Chapman & Hall, New York, 1988.
4 H. Ohigashi, S. Akama and K. Koga, Lamellar and Bulk Single Crystals Grown in Annealed Films of Vinylidene Fluoride and Trifluoroethylene Copolymers, *Jpn. J. Appl. Phys.*, 1988, **27**, 2144–2150.
5 G. T. Davis, J. E. McKinney, M. G. Broadhurst and S. C. Roth, Electric-field-induced phase changes in poly(vinylidene fluoride), *J. Appl. Phys.*, 1978, **49**, 4998–5002.
6 D. Yang and Y. Chen, β-phase formation of poly(vinylidene fluoride) from the melt induced by quenching, *J. Mater. Sci. Lett.*, 1987, **6**, 599–603.
7 M. A. Bachmann and J. B. Lando, A reexamination of the crystal structure of phase II of poly(vinylidene fluoride), *Macromolecules*, 1981, **14**, 40–46.
8 H. Kawai, The Piezoelectricity of Poly (vinylidene Fluoride), *Jpn. J. Appl. Phys.*, 1969, **8**, 975–976.
9 L. Zhang, Z. Liu, X. Lu, G. Yang, X. Zhang and Z. Y. Cheng, Nano-clip based composites with a low percolation threshold and high dielectric constant, *Nano Energy*, 2016, **26**, 550–557.
10 L. Zhang, X. Shan, P. Wu and Z. Y. Cheng, Dielectric characteristics of CaCu3Ti4O12/P(VDF-TrFE) nanocomposites, *Appl. Phys. A: Mater. Sci. Process.*, 2012, **107**, 597–602.
11 X. Liao, W. Ye, L. Chen, S. Jiang, G. Wang, L. Zhang and H. Hou, Flexible hdC-G reinforced polyimide composites with high dielectric permittivity, *Composites, Part A*, 2017, **101**, 50–58.
12 X. Lu, L. Zhang, Y. Tong and Z. Y. Cheng, BST-P(VDF-CTFE) nanocomposite films with high dielectric constant, low dielectric loss, and high energy-storage density, *Composites, Part B*, 2019, **168**, 34–43.
13 Y.-Y. Chiu, W.-Y. Lin, H.-Y. Wang, S.-B. Huang and M.-H. Wu, Development of a piezoelectric polyvinylidene

fluoride (PVDF) polymer-based sensor patch for simultaneous heartbeat and respiration monitoring, *Sens. Actuators, A*, 2013, **189**, 328–334.

14 P. Saketi, S. K. Latifi, J. Hirvonen, S. Rajala, A. Vehkaoja, T. Salpavaara, J. Lekkala and P. Kallio, PVDF microforce sensor for the measurement of Z-directional strength in paper fiber bonds, *Sens. Actuators, A*, 2015, **222**, 194–203.

15 V. Cauda, S. Stassi, K. Bejtka and G. Canavese, Nanoconfinement: an Effective Way to Enhance PVDF Piezoelectric Properties, *ACS Appl. Mater. Interfaces*, 2013, **5**, 6430–6437.

16 Q. Li, W. Ke, T. Chang and Z. Hu, A molecular ferroelectrics induced electroactive β-phase in solution processed PVDF films for flexible piezoelectric sensors, *J. Mater. Chem. C*, 2019, **7**, 1532–1543.

17 X. Lu, L. Hou, L. Zhang, Y. Tong, G. Zhao and Z. Y. Cheng, Piezoelectric-excited membrane for liquids viscosity and mass density measurement, *Sens. Actuators, A*, 2017, **261**, 196–201.

18 S. C. B. Mannsfeld, B. C. K. Tee, R. M. Stoltenberg, C. V. H. H. Chen, S. Barman, B. V. O. Muir, A. N. Sokolov, C. Reese and Z. Bao, Highly sensitive flexible pressure sensors with microstructured rubber dielectric layers, *Nat. Mater.*, 2010, **9**, 859–864.

19 S. Georgakopoulos, F. G. del Pozo and M. Mas-Torrent, Flexible organic transistors based on a solution-sheared PVDF insulator, *J. Mater. Chem. C*, 2015, **3**, 12199–12202.

20 P. E. Bloomfield and W. R. Scott, Measurement of the high frequency piezoelectric strain response of polarized PVDF, *Ferroelectrics*, 1984, **57**, 23–36.

21 E. Erdtman, K. C. Satyanarayana and K. Bolton, Simulation of α- and β-PVDF melting mechanisms, *Polymer*, 2012, **53**, 2919–2926.

22 W. A. Yee, M. Kotaki, Y. Liu and X. Lu, Morphology, polymorphism behavior and molecular orientation of electrospun poly(vinylidene fluoride) fibers, *Polymer*, 2007, **48**, 512–521.

23 A. J. Lovinger, Crystallization of the β phase of poly(vinylidene fluoride) from the melt, *Polymer*, 1981, **22**, 412–413.

24 K. C. Satyanarayana, M. Bohlén, A. Lund, R. W. Rychwalski and K. Bolton, Analysis of the torsion angle distribution of poly(vinylidene fluoride) in the melt, *Polymer*, 2012, **53**, 1109–1114.

25 M. Tamura, S. Hagiwara, S. Matsumoto and N. Ono, Some aspects of piezoelectricity and pyroelectricity in uniaxially stretched poly(vinylidene fluoride), *J. Appl. Phys.*, 1977, **48**, 513–521.

26 R. C. G. Naber, K. Asadi, P. W. M. Blom, D. M. de Leeuw and B. de Boer, Organic Nonvolatile Memory Devices Based on Ferroelectricity, *Adv. Mater.*, 2010, **22**, 933–945.

27 A. J. Lovinger, D. D. Davis, R. E. Cais and J. M. Kometani, The role of molecular defects on the structure and phase transitions of poly(vinylidene fluoride), *Polymer*, 1987, **28**, 617–626.

28 A. J. Lovinger, Crystallization and morphology of melt-solidified poly(vinylidene fluoride), *J. Polym. Sci., Polym. Phys. Ed.*, 1980, **18**, 793–809.

29 P. Güthner, T. Ritter and K. Dransfeld, Temperature dependence of the piezoelectric constant of thin PVDF and P(VDF-TrFE) films, *Ferroelectrics*, 1992, **127**, 7–11.

30 V. Strashilov, G. Alexieva, B. Vincent, V. S. Nguyen and D. Rouxel, Structural impact on piezoelectricity in PVDF and P(VDF-TrFE) thin films, *Appl. Phys. A: Mater. Sci. Process.*, 2015, **118**, 1469–1477.

31 L. Burianova, P. Hana, Y. I. Tyagur and J. Kulek, Piezoelectric hydrostatic coefficients of PVDF and P(VDF-TrFE) copolymer foils at high hydrostatic pressures, *Ferroelectrics*, 1999, **224**, 29–38.

32 A. J. Lovinger, G. E. Johnson, H. E. Bair and E. W. Anderson, Structural, dielectric, and thermal investigation of the Curie transition in a tetrafluoroethylene copolymer of vinylidene fluoride, *J. Appl. Phys.*, 1984, **56**, 2412–2418.

33 T. Yagi and M. Tatemoto, A Fluorine-19 NMR Study of the Microstructure of Vinylidene Fluoride–Trifluoroethylene Copolymers, *Polym. J.*, 1979, **11**, 429–436.

34 T. Yagi, M. Tatemoto and J.-i. Sako, Transition Behavior and Dielectric Properties in Trifluoroethylene and Vinylidene Fluoride Copolymers, *Polym. J.*, 1980, **12**, 209–223.

35 T. Furukawa, G. E. Johnson, H. E. Bair, Y. Tajitsu, A. Chiba and E. Fukada, Ferroelectric phase transition in a copolymer of vinylidene fluoride and trifluoroethylene, *Ferroelectrics*, 1981, **32**, 61–67.

36 K. Tashiro, H. Tadokoro and M. Kobayashi, Structure and piezoelectricity of poly(vinylidene fluoride), *Ferroelectrics*, 1981, **32**, 167–175.

37 L. Yang, X. Li, E. Allahyarov, P. L. Taylor, Q. M. Zhang and L. Zhu, Novel polymer ferroelectric behavior via crystal isomorphism and the nanoconfinement effect, *Polymer*, 2013, **54**, 1709–1728.

38 R. Su, J.-K. Tseng, M.-S. Lu, M. Lin, Q. Fu and L. Zhu, Ferroelectric behavior in the high temperature paraelectric phase in a poly(vinylidene fluoride-*co*-trifluoroethylene) random copolymer, *Polymer*, 2012, **53**, 728–739.

39 W. Xia, Z. Wang, J. Xing, C. Cao and Z. Xu, The Dependence of Dielectric and Ferroelectric Properties on Crystal Phase Structures of the Hydrogenized P(VDF-TrFE) Films With Different Thermal Processing, *IEEE Trans. Ultrason. Eng.*, 2016, **63**, 1674–1680.

40 J. L. Lutkenhaus, K. McEnnis, A. Serghei and T. P. Russell, Confinement Effects on Crystallization and Curie Transitions of Poly(vinylidene fluoride-*co*-trifluoroethylene), *Macromolecules*, 2010, **43**, 3844–3850.

41 W. M. Xia, Y. J. Gu, C. Y. You, C. J. Cao, Z. Xu and Z. C. Zhang, A crystal phase transition and its effect on the dielectric properties of a hydrogenated P(VDF-*co*-TrFE) with low TrFE molar content, *RSC Adv.*, 2015, **5**, 107557–107565.

42 R. I. Mahdi, W. C. Gan, W. H. Abd Majid, N. I. Mukri and T. Furukawa, Ferroelectric polarization and pyroelectric activity of functionalized P(VDF-TrFE) thin film lead free nanocomposites, *Polymer*, 2018, **141**, 184–193.

43 F. Guan, J. Pan, J. Wang, Q. Wang and L. Zhu, Crystal Orientation Effect on Electric Energy Storage in Poly(vinylidene fluoride-*co*-hexafluoropropylene) Copolymers, *Macromolecules*, 2010, **43**, 384–392.

44 Z. Zhang and T. C. M. Chung, The Structure–Property Relationship of Poly(vinylidene difluoride)-Based Polymers with Energy Storage and Loss under Applied Electric Fields, *Macromolecules*, 2007, **40**, 9391–9397.
45 Z. Zhang, Q. Meng and T. C. M. Chung, Energy storage study of ferroelectric poly(vinylidene fluoride-trifluoroethylene-chlorotrifluoroethylene) terpolymers, *Polymer*, 2009, **50**, 707–715.
46 R. Gregorio Jr, Determination of the α, β, and γ crystalline phases of poly(vinylidene fluoride) films prepared at different conditions, *J. Appl. Polym. Sci.*, 2006, **100**, 3272–3279.
47 L. Zhu, Exploring Strategies for High Dielectric Constant and Low Loss Polymer Dielectrics, *J. Phys. Chem. Lett.*, 2014, **5**, 3677–3687.
48 K. Koga, N. Nakano, T. Hattori and H. Ohigashi, Crystallization, field-induced phase transformation, thermally induced phase transition, and piezoelectric activity in P(vinylidene fluoride-TrFE) copolymers with high molar content of vinylidene fluoride, *J. Appl. Phys.*, 1990, **67**, 965–974.
49 J. S. Green, J. P. Rabe and J. F. Rabolt, Studies of chain conformation above the Curie point in a vinylidene fluoride/trifluoroethylene random copolymer, *Macromolecules*, 1986, **19**, 1725–1728.
50 E. Bellet-Amalric and J. F. Legrand, Crystalline structures and phase transition of the ferroelectric P(VDF-TrFE) copolymers, a neutron diffraction study, *Eur. Phys. J. B*, 1998, **3**, 225–236.
51 Y. Lu, J. Claude, Q. Zhang and Q. Wang, Microstructures and Dielectric Properties of the Ferroelectric Fluoropolymers Synthesized via Reductive Dechlorination of Poly(vinylidene fluoride-*co*-chlorotrifluoroethylene)s, *Macromolecules*, 2006, **39**, 6962–6968.
52 Z. Wang, Z. Zhang and T. C. M. Chung, High Dielectric VDF/TrFE/CTFE Terpolymers Prepared by Hydrogenation of VDF/CTFE Copolymers: Synthesis and Characterization, *Macromolecules*, 2006, **39**, 4268–4271.
53 K. Koga and H. Ohigashi, Piezoelectricity and related properties of vinylidene fluoride and trifluoroethylene copolymers, *J. Appl. Phys.*, 1986, **59**, 2142–2150.
54 H. Ohigashi, Electromechanical properties of polarized polyvinylidene fluoride films as studied by the piezoelectric resonance method, *J. Appl. Phys.*, 1976, **47**, 949–955.

